

# Relativistic electron energy loss and induced radiation emission in two-dimensional metallic photonic crystals. II. Photonic band effects

Tetsuyuki Ochiai and Kazuo Ohtaka

*Center for Frontier Science, Chiba University, Chiba 263-8522, Japan*

(Received 26 August 2003; published 18 March 2004)

This paper presents a fully relativistic analysis of the electron energy loss and the induced radiation emission in a metallic photonic crystal. The crystal's lattice constant is comparable with the plasma wavelength, and the analysis is presented in terms of the multiple scattering method based on vector cylindrical waves. The electron energy loss and the Smith-Purcell radiation emission spectra are well correlated with the photonic band structures, both with and without a structural defect. In particular, surface-localized modes and wave guide modes localized in a linear defect can be identified in the spectra. In addition, we show that highly directive radiation emission is possible by using a waveguide mode at the  $\Gamma$  point.

DOI: 10.1103/PhysRevB.69.125107

PACS number(s): 42.70.Qs, 73.20.Mf, 34.50.Bw

## I. INTRODUCTION

In the preceding paper<sup>1</sup> (referred to as Paper I) we presented a fully relativistic description of electron energy loss (EEL) and induced radiation emission in arbitrary arrays of nonoverlapping metallic cylinders. The description is given in terms of the multiple scattering method based on vector cylindrical waves. As an example, we have explored arrays of aluminum cylinders whose diameters are a few nanometers, considering carbon nanotube arrays and other metallic nanostructures. Using a nanoscale periodic structure, the induced radiation emission is prohibited kinetically in the frequency range of interest which is near the plasma frequency of aluminum. Thus, the EEL consists solely of the absorption in the structure. Moreover, an effective medium approximation can be reasonably applied to the structure because the wavelength is much greater than the pitch of the periodic structure.

However, if the diameter of the cylinders and the pitch in an array of metallic cylinders are comparable to or exceeds the plasma wavelength, the EEL and the induced radiation emission have a pronounced feature reflecting the photonic band structure. In particular, Smith-Purcell radiation (SPR) occurs in the frequency range of interest. As a consequence, a significant part of the EEL is caused by the SPR.

In this paper, we focus on the effects of photonic bands in a periodic array of metallic cylinders. As a model system, we choose a silver cylinder with radius  $r$  (160 nm) since silver has a low imaginary part in the dielectric function at the frequencies of visible light. Thus, we may expect that the absorption in the photonic crystal is quite small, so that the EEL is dominated by the SPR. The dielectric function of silver at these frequencies can be approximated with the following Drude formula:

$$\varepsilon_a(\omega) = \varepsilon_\infty - \frac{\omega_p^2}{\omega(\omega + i\eta)}, \quad (1)$$

where  $\varepsilon_\infty = 5.7$ ,  $\hbar\omega_p = 9$  eV, and  $\hbar\eta = 0.04$  eV. The surface plasmon polariton in a flat silver-air interface can be found at

$$\omega = \frac{\omega_p}{\sqrt{\varepsilon_\infty + 1}} \quad (2)$$

in the nonretardation limit. The above dielectric profile of silver, as well as copper and nickel, can be utilized as the ingredient of a three-dimensional photonic crystal with an omnidirectional band gap.<sup>2</sup> In fact, a dense face-centered cubic array of silver spheres with the same diameter has the complete photonic band gap far below the plasma frequency. Since the gap opens between the fifth and the sixth bands, it is robust against disorder. This is compared with the inverse opal, in which the complete band gap opens between the eighth and ninth bands.

This feature repeats in a dense square array of the silver cylinders in air. In contrast to metallic spheres, an array of metallic cylinders gives rise to polarization-sensitive light propagation because of the anisotropy of the structure. As is common knowledge, a periodic array of metallic cylinders behaves as if it is a bulk metal, with the low-frequency plasmon for the TM-polarized light,<sup>3</sup> whose electric field is parallel to the cylindrical axis, traveling in-plane perpendicular to the cylindrical axis. The plasma frequency of the low-frequency plasmon is roughly estimated as

$$\omega_c \simeq \sqrt{\frac{f}{1-f+f\varepsilon_\infty}} \omega_p, \quad (3)$$

$f$  being the filling fraction of the silver cylinders. Below  $\omega = \omega_c$  there is no bulk eigenmode of the TM polarization in the photonic crystal. For TE polarization, in which the magnetic field is parallel to the cylindrical axis, the photonic band structure has a wide band gap between the first and the second bands at  $k_z = 0$ . Therefore, the metallic photonic crystal has the polarization-independent in-plane gap as long as  $\omega_c$  exceeds the upper gap edge of the TE polarization. Owing to the band gap, a variety of localized defect modes may appear when structural defects are introduced. It is important to explore in detail what happens when a charged particle passes near a metallic photonic crystal with such a band gap. We address this issue in the present paper.

The paper is organized as follows. In Sec. II the photonic band structure of a metallic photonic crystal is studied in

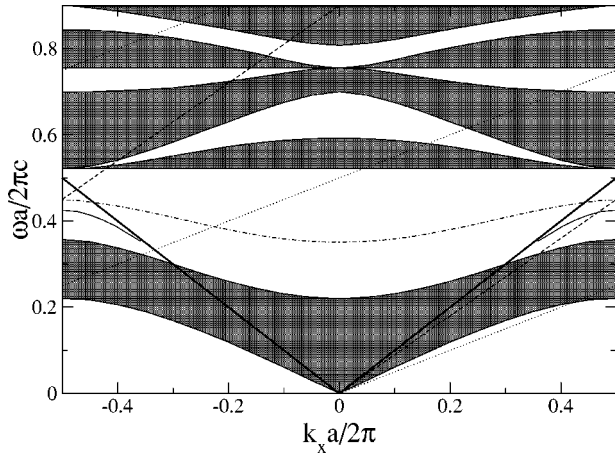


FIG. 1. The TE photonic band structure of the square lattice of the silver cylinders at  $k_z=0$  was projected onto the surface Brillouin zone associated with the boundary parallel to the (1,0) direction of the square lattice. The lattice constant is  $a=r/0.45 \approx 355.6$  nm, where  $r$  is the radius of the cylinders, which was taken to be 160 nm. The shaded regions correspond to the bulk eigenmodes, whereas the blank regions correspond to the (pseudo) gaps. The thick solid line is the light line ( $\omega = \pm ck_x$ ) and the dotted (dashed) lines are the  $v$  lines [ $\omega = v(k_x + h)$ ], which represent the dispersion of the radiation accompanied by the charged particle traveling with velocity  $v = 0.5c$  ( $0.9c$ ). The charged particle is supposed to travel parallel to the boundary of the photonic crystal. The dispersion curve of the surface-localized mode (discussed in Sec. III) and that of the wave guide mode, which is obtained by removing a single column of the cylinders from the photonic crystal (discussed in Sec. IV), are also shown (solid and dash-dotted lines).

connection with the SPR. We explore how the bulk eigenmodes as well as the surface-localized mode of the metallic photonic crystal affect the EEL and SPR spectra in Sec. III. Section IV discusses a possible scenario of directive SPR in the photonic crystal. Finally, we summarize the results.

## II. PHOTONIC BAND AND SMITH-PURCELL RADIATION

Photonic band effects play a crucial role in the EEL and SPR spectra in a photonic crystal, particularly in the frequency range comparable with the lattice scale. Here we study a metallic photonic crystals composed of a square array of silver cylinders with the lattice constant  $a = r/0.45 \approx 355.6$  nm. The photonic crystal is assumed to have infinite extent in the (1,0) direction of the square lattice and to have a finite thickness along the (0,1) direction. As in Paper I, the  $x$ ,  $y$ , and  $z$  axes are considered to be parallel to (1,0), (0,1), and the cylindrical axis, respectively. The photonic band structure of  $P$  (TE) polarization at  $k_z=0$  projected onto the surface Brillouin zone associated with the boundary parallel to (1,0) is shown in Fig. 1. The band structure was calculated by using the two-dimensional layer Korringa-Kohn-Rostoker-Ohtaka method taking  $l_{\max}=10$ . Here, we dropped the band diagram of the  $S$  (TM) polarization because it is not relevant to our problem. However, at nonzero  $k_z$  we must take account of both the  $S$  and  $P$  polarizations owing to polarization mixing. In Fig. 1 the shaded regions correspond

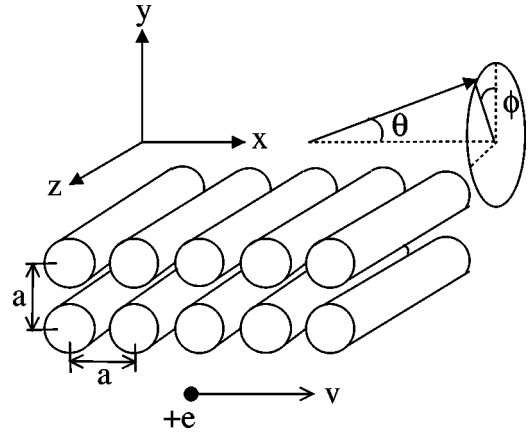


FIG. 2. Schematic illustration of the system under study. The photonic crystal has infinite extent in the  $xz$  plane and has a finite thickness along the  $y$  direction (just two layers in the figure). A charged particle travels below the photonic crystal and induces the Smith-Purcell radiation (SPR). The polar angle  $\theta$  of the SPR is defined as the inner angle between the unit vector directed to a far-field observation point and the  $x$  axis. The azimuthal angle  $\phi$  is defined on the  $yz$  plane. The  $y(z)$  axis corresponds to  $\phi = 0^\circ(90^\circ)$ .

to the bulk eigenmodes, whereas the blank regions correspond to the (pseudo) gaps. The photonic crystal has a large in-plane band gap between the first and the second bands. The gap-width/mid-gap ratio is about 36% at  $k_z=0$ . We should note that the in-plane band gap is polarization-independent because the cutoff frequency  $\omega_c$  for the TM polarization is about 0.92 in units of  $2\pi c/a$ . The in-plane gap, nevertheless, opens at small  $k_z$  even after mixing of the polarizations, whereas the gap increases in frequency. In addition, at high frequencies near  $\omega a/2\pi c = 1$ , there are infinite flat bands of surface plasmon polariton (SPP) origin. This is logical, taking into account that  $\omega_p/\sqrt{\epsilon_\infty + 1} = 0.997$  in units of  $2\pi c/a$ . The following discussion is restricted to the frequency region below  $\omega a/2\pi c \leq 0.9$ , such that the flat bands of SPP origin can be neglected.

Before discussing the effects of the photonic bands on the EEL and SPR, we should recall the kinetics involved in the EEL and SPR. A schematic illustration of the system under study is shown in Fig. 2. When a charged particle passes near the photonic crystal with its trajectory parallel to the (1,0) direction, the particle produces a source term of the external current in Maxwell's equation of the system. The term is proportional to  $\delta(x-vt)$ , where  $\delta$  is Dirac's  $\delta$  function. Therefore, the Fourier transform with respect to  $x$  and  $t$  yields the dispersion relation  $\omega = vk_x$  (referred to as the  $v$  line) for the radiation accompanied by the charged particle. In a vacuum, this dispersion is outside the light cone, and thus the radiation is evanescent. However, the radiation is scattered by the photonic crystal, acquiring an Umklapp momentum shift for  $k_x$  owing to the periodicity of the photonic crystal. After the scattering, the shifted  $v$  line  $\omega = v(k_x + h)$  lies partially inside the light cone. Here,  $h = (2\pi n)/a$ , where  $n$  is an integer) stands for a reciprocal lattice associated with the (1,0) direction. Therefore, the evanescent radiation can transform into a propagating one. In order to visualize this,

the  $v$  lines of different velocities ( $v=0.5c$  and  $0.9c$ ) and the light line  $\omega = \pm ck_x$  (provided  $k_z=0$ ) are overlaid onto the projected band structure in Fig. 1. As can be seen in Fig. 1, the shifted  $v$  line of  $v=0.5c$  and  $h=1$  in units of  $2\pi/a$  is inside the light cone if  $\omega a/2\pi c \geq 0.333$ . For the shifted  $v$  line of  $v=0.9c$  and  $h=1$ , the line is inside the light cone if  $\omega a/2\pi c \geq 0.474$ . In general, the shifted  $v$  line of velocity  $v$  and  $h=1$  is inside the light cone if the following condition is satisfied:

$$\frac{\omega a}{2\pi c} \geq \frac{\frac{v}{c}}{1 + \frac{v}{c}}. \quad (4)$$

This provides the low-frequency threshold of the SPR.

To describe the propagating direction of the SPR, it is convenient to introduce the polar coordinate (Fig. 2). The polar angle  $\theta$  is defined as the inner angle between the unit vector directed to a far-field observation point and the  $x$  axis. The azimuthal angle  $\phi$  is defined on the  $yz$  plane. Since the  $x$  component of the wave number vector of the SPR is given by  $k_x = \omega/v - h$ , the polar angle of the SPR is fixed as

$$\cos \theta_h = \frac{\frac{\omega}{v} - h}{\frac{\omega}{c}}, \quad (5)$$

at a given frequency  $\omega$ . The azimuthal angle of the SPR depends on both  $\omega$  and  $k_z$ , and is given by

$$\tan \phi = \frac{k_z}{\sqrt{\left(\frac{\omega}{c}\right)^2 - \left(\frac{\omega}{v} - h\right)^2 - k_z^2}}. \quad (6)$$

Since the  $k_z$  integral is involved in the SPR spectrum, as was derived in Paper I, the azimuthal angle of the SPR is not fixed.

In the photonic crystal we must combine the above kinetics with the photonic dispersion relation  $\omega = \omega_n(k_x, k_y, k_z)$  inside the crystal. We can expect that a large enhancement of the EEL and SPR when the  $v$  lines (including the shifted ones) hit the photonic bands. This is caused by exciting photonic eigenstates on the  $v$  lines. As depicted in Fig. 1, the  $v$  lines are partially in the shaded regions that correspond to the bulk eigenstates and are also in the pseudogaps. The shaded region does not truly represent a continuous distribution of photonic eigenstates. Rather, it represents a dense but discrete distribution of them. This is due to our using a finite-thickness photonic crystal, and the quantization of the momentum along the direction of thickness must be considered. Therefore, by scanning  $\omega$ , the  $v$  lines hit a sequence of discrete-level eigenstates. Thus, the EEL and SPR spectra reveal a rapid oscillation inside the shaded regions. Let us suppose that one of the eigenstates on the  $v$  line causes a strong enhancement in the SPR spectrum. This yields a monochromatic radiation with a particular frequency, and

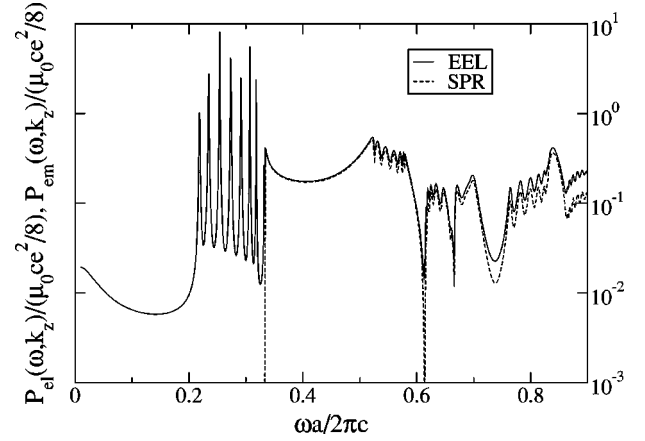


FIG. 3. The EEL (solid line) and SPR (dashed line) spectra in the eight-layer-thick photonic crystal under consideration (See the caption of Fig. 1). The charged particle travels with velocity  $v = 0.5c$ , maintaining a distance of  $0.5a$  from the plane bisecting the boundary layer.  $k_z=0$  was assumed.

thus the radiation is directed to a certain polar angle determined by Eq. (5). However, it does not generally imply that the radiation is also directive as it relates to the azimuthal angle. In Sec. IV, we will discuss how to obtain a directive SPR relating to both polar and azimuthal angles.

### III. BULK AND SURFACE STATES

Let us consider the EEL and SPR when a charged particle passes near the finite-thickness photonic crystal. In Fig. 1 the  $v$  lines of  $v=0.5c$  lie in the shaded region of the lowest band at  $0.2 \leq \omega a/2\pi c \leq 0.33$ . The lines are inside the photonic band gap in the frequency region between  $\omega a/2\pi c \approx 0.33$  and  $0.52$  and in the pseudogaps near  $\omega a/2\pi c \approx 0.6, 0.73$  and  $0.85$ . In contrast, the  $v$  lines of  $v=0.9c$  lie in the shaded region of the lowest band up to  $\omega a/2\pi c \approx 0.33$ . The lines are also inside the photonic band gap and in the three pseudogaps near  $\omega a/2\pi c = 0.53, 0.73,$  and  $0.8$ . Inside the band gap, the  $v$  line of  $v=0.9c$  lies partially outside the light cone.

As was mentioned, when the  $v$  line lies in a shaded region, the charged particle excites a sequence of bulk discrete-level eigenmodes in the region. Thus, the EEL and the SPR spectra reveal a rapid oscillation. Figure 3 shows both of these spectra in the eight-layer-thick photonic crystal along the  $(0,1)$  direction, where  $v=0.5c$  and  $k_z=0$  were assumed. The distance between the trajectory of the charged particle and the plane bisecting the boundary layer is  $0.5a$ . As was derived in Paper I, the two spectra must coincide if there is to be no absorption in the photonic crystal. Owing to the small imaginary part in the dielectric function of silver, the EEL spectrum is nearly equal to the SPR spectrum in a wide frequency region including the band gap. Below the threshold of the SPR the EEL spectrum has a sequence of very sharp peaks that appear when the  $v$  line lies in the shaded region of the lowest band in Fig. 1. Since this happens at rather low frequencies, an effective medium approximation is plausibly applied, so that the positions of these peaks can be estimated

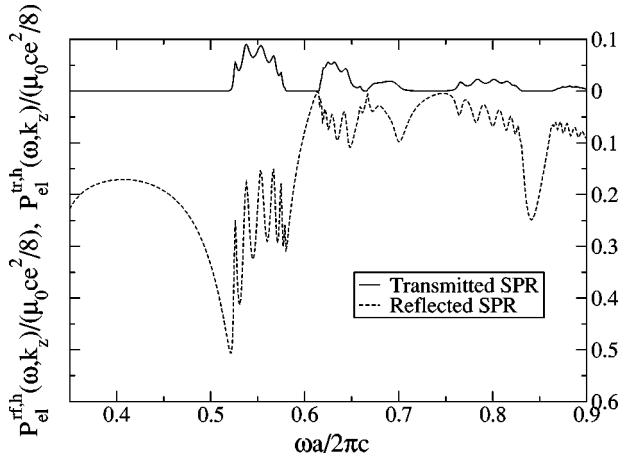


FIG. 4. Transmitted and reflected SPR spectra of Umklapp shifted channel  $h=1$  in the eight-layer-thick photonic crystal under study. The transmitted (reflected) SPR spectrum is shown above (below) the horizontal axis. The same parameters as in Figs. 1 and 2 were used.

by the same procedure used in Paper I. Above the SPR threshold, both spectra reveal a rich structure. At approximately  $\omega a/2\pi c=0.4$ , where the in-plane gap opens, the spectra have no pronounced structure. Moreover, one can find a marked dip at  $\omega a/2\pi c \approx 0.61$ , where a pseudogap opens. Here, the deviation of the SPR from the EEL is quite pronounced. Generally, above the threshold, this deviation becomes large at high frequencies even if the  $v$  line is in the shaded regions.

Though the band gap and the pseudogap can be identified in the EEL and the SPR spectra, their effects can be clearly demonstrated when we divide the SPR spectrum into the transmitted and reflected SPR spectra with fixed  $h$ , with focus on the transmitted spectrum. The transmitted and reflected SPR spectra are defined by

$$P_{\text{em}}(\omega, k_z) = \sum_{h \in \text{open}} [P_{\text{em}}^{\text{tr},h}(\omega, k_z) + P_{\text{em}}^{\text{rf},h}(\omega, k_z)], \quad (7)$$

$$P_{\text{em}}^{\text{tr},h}(\omega, k_z) = \frac{1}{8} \mu_0 e^2 \omega e^{-2|\gamma_{h_0}|s} \gamma_h |Q_{++}(h, h_0) \epsilon^+|^2, \quad (8)$$

$$P_{\text{em}}^{\text{rf},h}(\omega, k_z) = \frac{1}{8} \mu_0 e^2 \omega e^{-2|\gamma_{h_0}|s} \gamma_h |Q_{-+}(h, h_0) \epsilon^+|^2, \quad (9)$$

$$\gamma_h = \sqrt{\left(\frac{\omega}{c}\right)^2 - (k_x + h)^2 - k_z^2}, \quad (10)$$

where  $Q_{\pm\pm}$  is the scattering matrix of the finite-thickness photonic crystal,  $\epsilon^+$  is the plane-wave coefficient of the incident evanescent wave accompanied by the charged particle, and  $\omega/v$  is divided into the momentum in the first Brillouin zone  $k_x$  and a reciprocal lattice  $h_0$  (See Paper I for details).

Figure 4 shows both the transmitted and reflected SPR spectra for the same structure as in Fig. 3. As illustrated in Fig. 4, the transmitted SPR spectrum is almost zero in the gap and the pseudogaps. However, this does not imply that the reflected SPR spectrum has a peak there, because the total SPR spectrum is a complicated function of frequency.

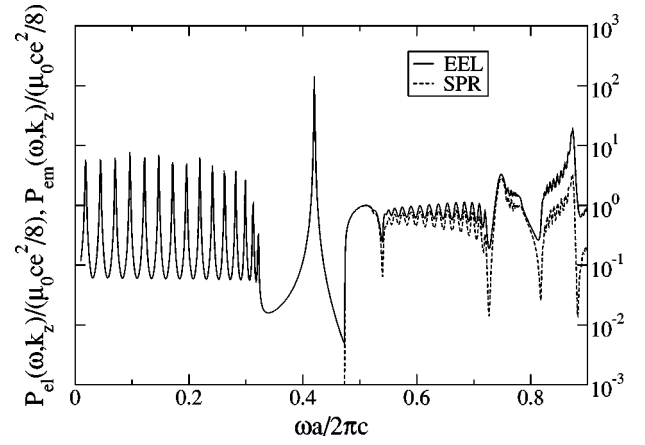


FIG. 5. EEL and SPR spectra in the 32-layer-thick photonic crystal along the (0,1) direction. The charged particle travels with velocity  $v=0.9c$ , maintaining distance  $0.5a$  from the plane bisecting the boundary layer.

Instead, the reflected SPR spectrum has no rapid oscillation in these gaps. Apparently, the transmitted SPR intensity decreases as the number of layers increases owing to light absorption. In contrast, the reflected SPR spectrum converges to a certain function as the number increases.

In Figs. 3 and 4, there is another dip at  $\omega a/2\pi c \approx 0.67$ , which does not correspond to any pseudogap in the photonic band structure. In fact, the dip is located inside the shaded region in Fig. 1. The dip appears at the intersection of the shifted  $v$  line of  $h=1$  and the line of the Bragg diffraction threshold ( $\omega = -ck_x + 2\pi/a$ ). Thus, the dip is somehow related to the Rayleigh-Wood anomaly of diffraction grating.<sup>4</sup>

In the band gap, the  $v$  lines may intersect the dispersion curve of a surface-localized mode on the interface between the photonic crystal and air. This is the case for the structure under consideration. As shown in Fig. 1, the  $v$  line of  $v=0.9c$  lies outside the light cone in the band gap, so that it can excite a surface-localized mode. Fig. 5 shows both the EEL and the total SPR spectra in the 32-layer-thick photonic crystal, where the charged particle travels with velocity  $v=0.9c$ . There is a remarkable peak of the EEL spectrum at  $\omega a/2\pi c \approx 0.42$ . The peak is higher than any other peaks found in the shaded region. Since the peak is found in the in-plane band gap outside the light cone, the peak is attributed to the surface-localized mode. By changing the velocity of the charged particle, we can trace the dispersion curve of the surface mode. The result was already implemented in Fig. 1. With this analysis, the electron energy loss spectroscopy is capable of experimentally determining the dispersion relation of the surface-localized mode.

#### IV. DIRECTIVE SMITH-PURCELL RADIATION

In the previous sections, we studied the effects of photonic bands on the EEL and SPR spectra in a finite-thickness photonic crystal. There, the spectra were compared with the projected band diagram, which is obtained from the photonic bands of the corresponding infinitely thick sample along the stacking direction. In the eight- or 32-layer thick samples,

fine structures of the EEL and SPR spectra can be clearly observed. However, as the number of layers increases, the fine structures become hidden, owing to the nonzero imaginary part of the dielectric function of silver. As a result, no marked peak of high quality can be found in the SPR spectrum of the thick samples, whereas the EEL spectrum still has the very sharp peak of the surface-localized mode. In view of coherent light source, it is advantageous to have a sharp peak in the SPR spectrum at a particular frequency. Moreover, the SPR is more useful when highly directive.

When we consider the photonic band structure in bulk, the wave vectors of the matched eigenstates to the charged particle are distributed on a surface in the first Brillouin zone because the matching condition is given by

$$\omega = \omega_n(k_x, k_y, k_z), \quad (11)$$

$$k_x = \frac{\omega}{v} \left( \text{mod} \frac{2\pi}{a} \right), \quad (12)$$

which generally has a two-dimensional solution in the momentum space. Therefore, it is difficult to realize a directive SPR in a thick sample.

The above difficulty can be overcome either by considering a monolayer of silver or by introducing a linear defect into the photonic crystal. In the former case, we can no longer adapt the concept of the projected band structure because it assumes infinite thickness along the stacking direction. Instead, the band structure of the quasiguided modes with finite lifetimes must be taken into account. The modes have a two-dimensional dispersion relation  $\omega = \omega_n(k_x, k_z)$  in which confinement of light in the  $y$  direction removes the  $k_y$  dependence in  $\omega_n$ . In the latter case, the linear defect can support a wave guide mode localized in it. The wave guide mode also has the two-dimensional dispersion relation. As a result, the wave vectors of the matched eigenstates in these structures are distributed on a curve in the first Brillouin zone. Thus, it is simple to have a directive SPR.

First, let us consider the monolayer case. Figure 6 illustrates the photonic band structure of the quasiguided modes in the light cone as well as the true guided modes outside the light cone. Again, we set  $k_z = 0$  for simplicity. The quasiguided modes in the figure were identified with the method given in Ref. 5, whereas the true guided modes were obtained by solving the secular equation  $\det(S^{-1}) = 0$ , where  $S$  is the scattering matrix of the monolayer. It should be stressed that if the shifted  $v$  line hits a quasiguide mode at the  $\Gamma$  point, it yields a directive SPR emission normal to the monolayer as long as no Bragg channels open. This scenario of the directive radiation emission is the same as that in dipole radiation,<sup>6</sup> where very high directivity is achieved by exciting a quasiguide mode at the  $\Gamma$  point.

To explore the directivity of the SPR in the monolayer, the elastic differential cross section is introduced. At a far-field observation point specified by solid angle  $\Omega = (\theta, \phi)$  (see Fig. 2), the only plane-wave components that contribute to the differential cross section at  $\Omega$  are those with the wave vector parallel to the solid angle. Thus, the elastic differential cross section of the SPR is given by

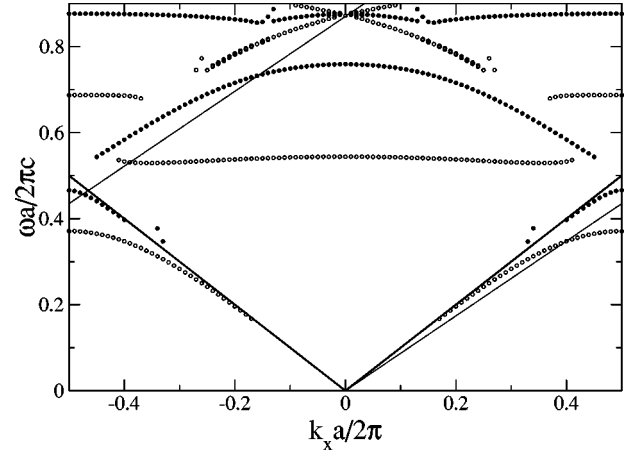


FIG. 6. Photonic band structure in the monolayer of silver cylinders. The same parameters as Fig. 1 were assumed. The open (solid) circles are the even (odd) modes with respect to the plane bisecting the monolayer. The thick solid line represents the boundary of the light cone; the thin solid line is the  $v$  line of  $v = 0.87c$ .

$$\frac{dP}{d\phi} = \cos^2 \phi \sin^2 \theta_h |\mathbf{t}_h^+(\omega, k_z)|^2, \quad (13)$$

per unit azimuthal angle. Here, since the polar angle of the propagating direction is fixed as in Eq. (5) in the SPR, the polar angle dependence of the differential cross section, which is given by a Dirac's  $\delta$  function at  $\theta = \theta_h$ , was integrated out. In Eq. (13),  $\mathbf{t}_h^+$ , which stands for the plane-wave coefficient of the electric field above the photonic crystal, has argument  $k_z$  equal to  $(\omega/c) \sin \theta_h \sin \phi$ .

In order to attain a directive SPR normal to the monolayer,  $\theta_h$  must be equal to  $90^\circ$ .<sup>7</sup> This can be achieved by imposing  $\omega/v = h$  and by taking  $\omega$  to be the frequency  $\omega_\Gamma$  of one of the quasiguided modes at the  $\Gamma$  point. For instance, putting  $v = \omega_\Gamma a / 2\pi n$  (where  $n$  is an integer) yields  $\theta_h = 90^\circ$  for the channel of  $h = n$  in units of  $2\pi/a$ . We should note, however, that at a typical velocity of the electron used in the EEL spectroscopy in a scanning transmission electron microscope ( $v \approx 0.5c$ ), only the channel of  $h = 1$  (in units of  $2\pi/a$ ) is favorable for the directive SPR. This is because in the frequency region relevant to the higher channels of  $h \geq 2$  the photonic band structure is so dense in frequency that we will not be able to obtain the SPR of monotonic frequency. In the following discussion we thus restrict ourselves to the channel of  $h = 1$ .

As presented in Fig. 6, the quasiguided modes appear at  $\omega a / 2\pi c = 0.544, 0.759, \text{ and } 0.870\text{--}0.877$ . However, the lower two modes yield very broad peaks in the SPR spectrum, reflecting that the corresponding peaks of the optical density of state are very broad in frequency. In contrast, the latter three modes combined yield a sharp peak in the SPR spectrum. Thus, we may expect a directive SPR normal to the monolayer to take place.

The scattering cross section of the SPR at  $\omega a / 2\pi c = 0.870$ , provided  $v = 0.870c$ , is shown in Fig. 7. In this case, the directivity of the SPR is not so high owing to the rather flat dispersions of the relevant quasiguide modes

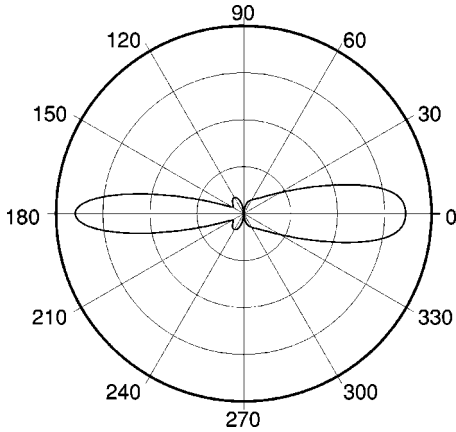


FIG. 7. The azimuthal angle ( $\phi$ ) distribution of the SPR in the monolayer of the silver cylinders. The velocity of the charged particle and the frequency were taken to be  $v=0.870c$  and  $\omega a/2\pi c=0.870$ , in order to excite the quasiguide mode at the  $\Gamma$  point. The distance between the trajectory of the charged particle and the plane bisecting the monolayer is  $0.5a$ .

along  $k_z$ . Furthermore, two small peaks of the angular distribution of the differential cross section are observed at  $\phi \approx 120^\circ$  and  $240^\circ$  in the reflected SPR. They represent the simultaneous excitation of another quasi-guided mode. In fact, we found that the band that terminates the quasi-guided mode of  $\omega a/2\pi c=0.759$  at  $k_z=0$  intersects the line of  $\omega a/2\pi c=0.870$  near the light line  $\omega = ck_z$ . The quasi-guide mode at the intersection is responsible for the small peaks. Therefore, in order to obtain directive SPR using the quasiguide modes, the dispersion of the quasiguide mode must be optimized.

Next, we consider a linear defect introduced in the silver photonic crystal employed in the preceding section. We first assume a nine-layer-thick photonic crystal, i.e., a stack of nine identical monolayers of the cylinders. We then remove the fifth layer altogether, leaving the linear defect parallel to the  $xz$  plane, which is sandwiched by four layers on each side. The resultant EEL and SPR spectra reveal a sharp resonance at the frequency of the wave guide mode. Thus, by tracking the peak frequencies as a function of  $k_x$  and  $k_z$ , we can determine the dispersion relation of the waveguide mode. The dispersion curve obtained in this way is plotted in Fig. 1. Moreover, an ordinary transmission calculation across the linear defect can also determine the dispersion curve in the light cone.<sup>8</sup> We have examined both methods, and the results are wholly consistent. As seen in Fig. 1, the dispersion curve lies mostly in the light cone, so that the SPR spectrum is strongly affected by the waveguide mode.

A waveguide mode can also be utilized for directive SPR because it also has a two-dimensional dispersion relation. It should be stressed here that the in-plane gap shifts upward in frequency with increasing  $|k_z|$ . The dispersion curve of the waveguide mode behaves similarly, as will be seen later. Moreover, the  $\Gamma$  point is a minimum as a function of  $k_x$ . This yields the dispersion relation approximated around  $(k_x, k_z) = (0, 0)$  with

$$\omega = \omega_0 + \alpha k_x^2 + \beta k_z^2 \quad (\alpha, \beta > 0), \quad (14)$$

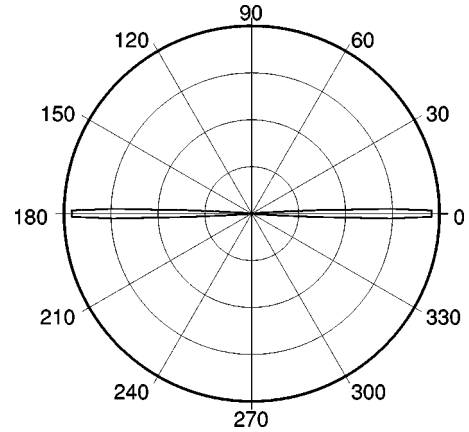


FIG. 8. The azimuthal angle  $\phi$  distribution of the SPR in the photonic crystal with a linear defect. The velocity of the charged particle and the frequency were taken to be  $v=0.351c$  and  $\omega a/2\pi c=0.351$ , in order to excite the waveguide mode at  $(k_x, k_z) = (0, 0)$ . The SPR is highly directive, compared with the monolayer case.

$\omega_0$  being the eigenfrequency of the waveguide mode at  $(k_x, k_z) = (0, 0)$ . When  $\omega$  and  $v$  are chosen such that  $\omega = \omega_0$  and  $k_x = 0, k_z = 0$  is also derived. Thus, the shifted  $v$  line only hits the waveguide mode at  $k_x = k_z = 0$  at this frequency. This yields a highly directive emission of SPR toward  $(\theta, \phi) = (90^\circ, 0^\circ)$ .

A similar directive radiation emission was studied in connection with the antenna application. Temelkuran *et al.*, reported that by introducing a planar defect in a woodpile structure with a complete photonic band gap, highly directive dipole radiation is achieved with the aid of the resonance of the planar defect mode.<sup>9</sup>

The scattering cross section of the SPR at  $\omega a/2\pi c = 0.351$ , which corresponds to the waveguide mode at

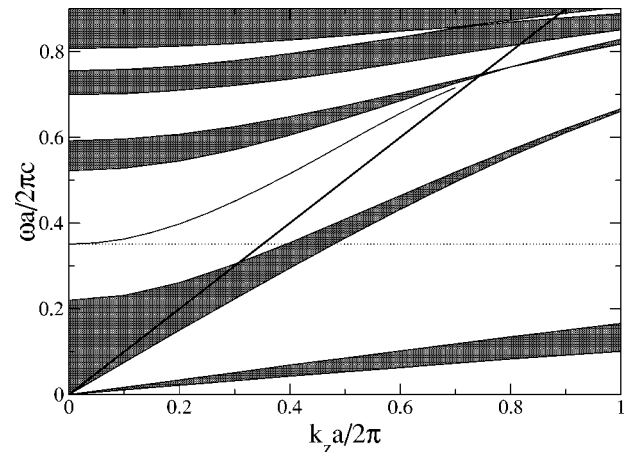


FIG. 9. The photonic band structure of the square photonic crystal under consideration (See Fig. 1 caption) is projected onto the  $k_z$  axis, provided  $k_x=0$ . The shaded regions correspond to the bulk eigenmodes, whereas the blank regions correspond to the (pseudo) gaps. The thick solid line is the light line  $\omega = ck_z$  and the thin solid line stands for the dispersion relation of the waveguide mode localized in the linear defect of a missing column. The dotted line is of  $\omega a/2\pi c=0.351$ .

$(k_x, k_z) = (0, 0)$  (the value of the dash-dotted curve at  $k_x = 0$  in Fig. 1), is shown in Fig. 8. Here, we assumed that the charged particle travels with velocity  $v = 0.351c$  inside the linear defect, keeping the same distance from the layers that sandwich the defect. In this case, only a wave guide mode with even parity with respect to the trajectory can be excited because of the even symmetry of the incident evanescent wave accompanied by the charged particle. In addition, the upper and lower transmitted SPR's are identical. As depicted in Fig. 8, the azimuthal angle distribution of the cross section is especially concentrated around  $\phi = 0^\circ$  (transmitted) and  $180^\circ$  (reflected). The high concentration is caused by the fact that there is no matched bulk eigenstate inside the light cone other than the wave guide mode at  $(k_x, k_z) = (0, 0)$ . This can be clearly seen in Fig. 9. In this figure the photonic band structure is projected onto the  $k_z$  axis provided  $k_x = 0$ , that is, the  $\Gamma$  point of the surface Brillouin zone. Outside the light cone the frequency  $\omega a/2\pi c = 0.351$  is matched to the bulk eigenmodes, which cannot couple to external radiation. Though these modes cause light absorption in the photonic crystal, the emitted light of the SPR is highly directive at that frequency.

## V. SUMMARY

In this paper, we analyzed how photonic bands affect the EEL and SPR spectra in a two-dimensional metallic photonic

crystal composed of silver cylinders whose plasma wavelength is comparable with the lattice constant. The spectra are well correlated with the photonic band structure of the sample with and without a structural defect. In particular, photonic band gaps, pseudogaps, surface-localized modes, and wave guide modes in the spectra can be identified. Thus, the EEL spectroscopy and the SPR measurement in a scanning transmission electron microscope provide an experimental method to determine such gaps and modes. However, possible fine structures in these spectra are hidden in a thick sample because of a nonzero imaginary part in the dielectric function of silver. This precludes the use of the SPR as a coherent light source in regular metallic photonic crystals. We proposed two routes to avoid this problem. One is to use the monolayer of the cylinders; the other is to use a linear defect introduced in the metallic photonic crystal. In both cases, we can obtain highly directive SPR's by tuning the frequency as well as the velocity of the charged particle.

## ACKNOWLEDGMENTS

This work was supported by the program "Promotion of Science and Technology" of the Ministry of Education, Sports, Culture, Science and Technology of Japan.

<sup>1</sup>T. Ochiai and K. Ohtaka, preceding paper, Phys. Rev. B **69**, 125106 (2004).

<sup>2</sup>Z. Wang, C.T. Chan, W. Zhang, N. Ming, and P. Sheng, Phys. Rev. B **64**, 113108 (2001).

<sup>3</sup>J.B. Pendry, A.J. Holden, W.J. Stewart, and I. Youngs, Phys. Rev. Lett. **76**, 4773 (1996).

<sup>4</sup>Lord Rayleigh, Proc. R. Soc. London, Ser. A **79**, 399 (1907).

<sup>5</sup>K. Ohtaka, Y. Suda, S. Nagano, T. Ueta, A. Imada, T. Koda, J.S. Bae, K. Mizuno, S. Yano, and Y. Segawa, Phys. Rev. B **61**, 5267

(2000).

<sup>6</sup>T. Ochiai and K. Ohtaka (unpublished).

<sup>7</sup>Observation with  $\theta = \theta_i = 90^\circ$  is the easiest from the experimental point of view.

<sup>8</sup>T. Ueta, K. Ohtaka, N. Kawai, and K. Sakoda, J. Appl. Phys. **84**, 6299 (1998).

<sup>9</sup>B. Temelkuran, M. Bayindir, E. Ozbay, R. Biswas, M.M. Sigalas, G. Tuttle, and K.M. Ho, J. Appl. Phys. **87**, 603 (2000).